

HELMHOLTZ DECOMPOSITION BASED ON INTEGRAL EQUATION METHOD FOR ELECTROMAGNETIC ANALYSIS

Xiaoyan Y. Z. Xiong, Wei E. I. Sha, and Li Jun Jiang

Department of Electrical and Electronic Engineering, The University of Hong Kong, Pokfulam, Hong Kong; Corresponding author: jianglj@hku.hk

Received 20 December 2013

ABSTRACT: Helmholtz decomposition (HD) is a vector analysis fundamental tool and plays an important role in electromagnetics (EM) and microwave engineering. Instead of applying HD to the EM solving process, this article proposes an integral equation based rigorous HD process to extract and analyze the known EM field. It provides much clearer insight into field coupling and radiation mechanism that is valuable to electromagnetic interference (EMI) and electromagnetic compatibility (EMC) analysis. Compared to the loop-tree based decomposition that is a quasi-HD, the proposed method is rigorous and frequency-independent. The algorithm verification and its application to coupling and resonating problems are presented. This method can provide a novel angle for the EM field analysis used in EMI/EMC, antennas, signal integrity, and relevant areas. © 2014 Wiley Periodicals, Inc. *Microwave Opt Technol Lett* 56:1838–1843, 2014; View this article online at wileyonlinelibrary.com. DOI 10.1002/mop.28454

Key words: Helmholtz decomposition; integral equation; wave and circuit physics; loop-tree decomposition

1. INTRODUCTION

Vector field analysis is fundamentally important in fields of mathematics, physics, and engineering. The Helmholtz's theorem [1] states that any sufficiently smooth, decaying vector field in three dimensions can be decomposed into the sum of a curl-free (CF)/irrotational and a divergence-free (DF)/solenoidal vector components. The Helmholtz decomposition (HD) could capture field features, such as sources, sinks, and vortices [2]. Thus, it is a powerful visual tool in several applications involving aerodynamic design, detection of flow features, computer graphics, and so forth [3]. This theorem is also of great importance in electromagnetic (EM) and microwave engineering, especially for solving the low-frequency breakdown issues caused by the decoupling of electric and magnetic fields. The loop-tree method, a quasi-HD based approach, was popularly used in solving low-frequency electric field integral equations (EFIE) [4].

Surprisingly, after solving the loop-tree from EFIE, it is not convenient to use them for the irrotational and solenoidal current representation and analysis. The reason is that it is not a rigorous decomposition and the tree basis is not CF. Hence, the irrotational current represented by the tree basis is not the true irrotational current. Plotting the current represented by the tree basis could be very messy with no valuable information for use. The rotational current analysis is also jeopardized because of this reason. Plus, this problem becomes worse when the frequency goes high. Because the solenoidal and irrotational components of the field contain very rich EM coupling and radiation information, it is important to have a convenient process to extract them rigorously from the given field. It would greatly benefit analysis and optimization of electromagnetic interference (EMI), antennas, signal integrity (SI), and so forth.

In this article, we develop an integral equation (IE) based method to numerically implement a rigorous HD process for the

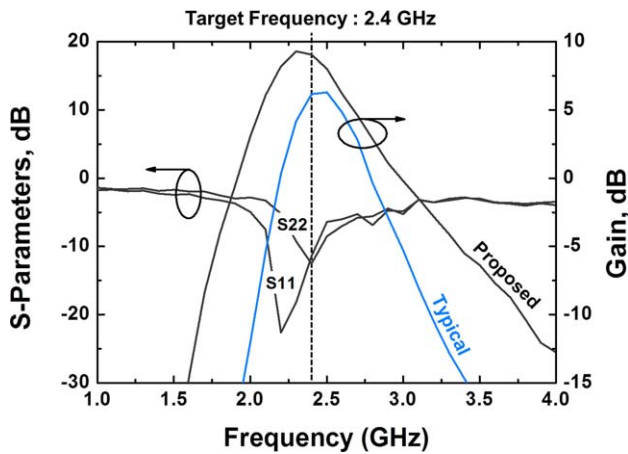


Figure 4 Measured *S*-parameters and gain of a typical and the proposed LNAs. [Color figure can be viewed in the online issue, which is available at wileyonlinelibrary.com]

technique, a shunt inductor at the input and a source degeneration inductor are laid out so that the current directions of the adjacent metal lines are equal. Accordingly, the magnetic coupling between the two inductors enhances the inductance levels of the two inductors due to the mutual inductance. To verify the feasibility of the proposed technique, we designed a 2.4-GHz differential LNA using 0.13- μm RFCMOS technology. Using the proposed technique, the chip size is reduced to 68% of a typical LNA. According to the measured results, we successfully prove that the gain and NF of the proposed LNA are improved compared to those of a typical LNA.

ACKNOWLEDGMENT

This work was supported by a grant from the National Research Foundation of Korea (NRF) funded by the Korean government (MEST) (No. 20110020262).

REFERENCES

1. C. Park, D.H. Lee, S.-H. Baek, Y. Kim, and S. Hong, 1.8-GHz CMOS power amplifier with stage-convertible structure using differential line inductor, *IEEE Radio Frequency Integrated Circuits Symposium*, Honolulu, 2007, pp. 741–744.
2. J. Park, C. Lee, and C. Park, A brief review: stage-convertible power amplifier using differential line inductor, *Wireless Eng Technol* 3 (2012), 189–194.
3. Y.S. Wang and L.-H. Lu, 5.7 GHz low-power variable-gain LNA in 0.18 μm CMOS, *Electron Lett* 41 (2005), 66–68.
4. M.-H. Tasi, S.S.H. Hsu, F.-L. Hsueh, C.-P. Jou, and T.-J. Yeh, A 17.5–26 GHz low-noise amplifier with over 8 kV ESD protection in 65 nm CMOS, *IEEE Microwave Wireless Compon Lett* 22 (2012), 483–485.
5. J.-H. Wu and C.-H. Yeh, A GPS LNA RFIC with voltage-controlled noise and input matching, *Microwave Opt Technol Lett* 54 (2012), 332–335.
6. A. Iji, X. Zhu, and M. Heimlich, Low power, high gain, low noise amplifier (LNA) for ultra wide band applications, *Microwave Opt Technol Lett* 55 (2013), 1399–1401.
7. A. Iji, X. Zhu, and M. Heimlich, A 4.5 mW 3–5 GHz low-noise amplifier in 0.25- μm silicon-on-insulator CMOS process for power-constraint application, *Microwave Opt Technol Lett* 55 (2013), 89–93.

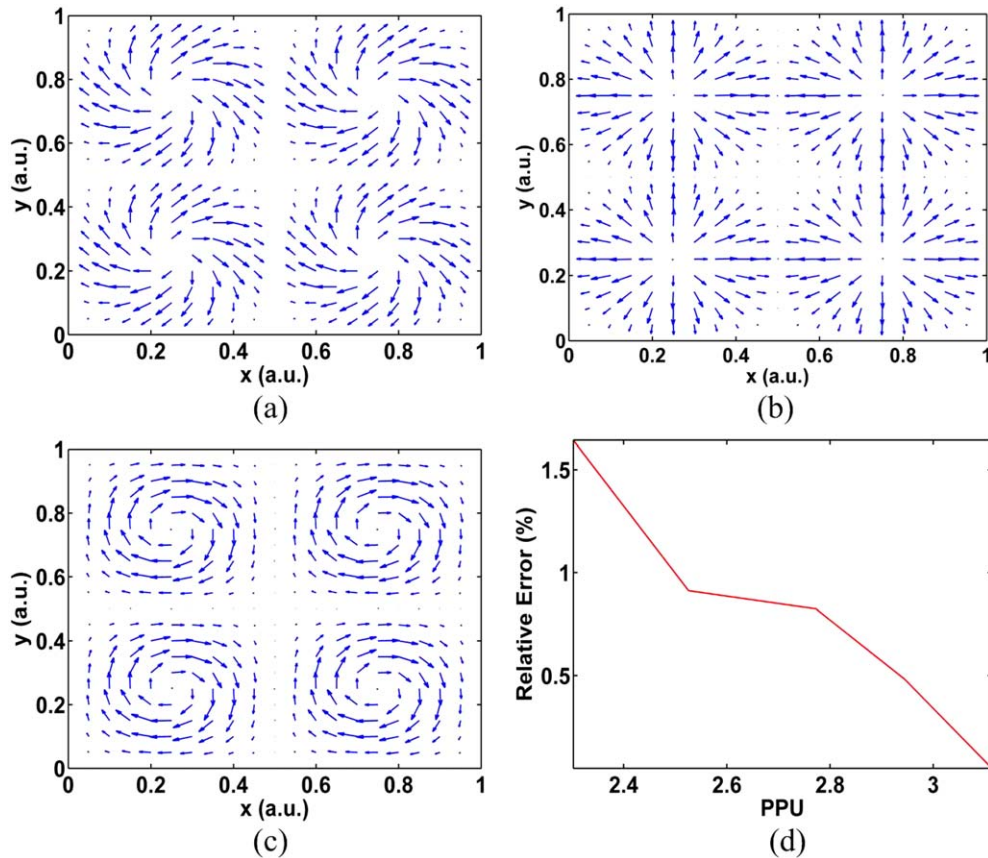


Figure 1 The HD of a fictitious vector current on the planar surface based on the SIE. (a) The original current; (b) the CF current; (c) the DF current; and (d) the relative errors of the CF currents as a function of points per unit and the wave number. [Color figure can be viewed in the online issue, which is available at wileyonlinelibrary.com]

EM field on a simply-connected planar surface. To demonstrate the difference of the proposed method compared to the loop-tree decomposition, and to show its practical applications, we applied it to the EMI analysis of transmission lines and the working status analysis of a resonator. From the results, it is clear that the proposed method provides very new and much more physical interpretation than regular total current or field.

2. THEORY

2.1. HD for a Planar Surface

Assume the given electric or magnetic current density is \mathbf{S} . If it is bounded and approaches zero at large distances, according to the Helmholtz' theorem, we can decompose it into a DF part \mathbf{S}^{div} and a CF part \mathbf{S}^{curl}

$$\mathbf{S} = \mathbf{S}^{\text{div}} + \mathbf{S}^{\text{curl}} \quad (1)$$

It has been shown that \mathbf{S}^{div} and \mathbf{S}^{curl} could be constructed explicitly as follows [5]

$$\mathbf{S}^{\text{div}} = \frac{1}{4\pi} \nabla \times \int_{V'} \frac{\nabla' \times \mathbf{S}(\mathbf{r}')}{|\mathbf{r} - \mathbf{r}'|} d\mathbf{r}' \quad (2)$$

$$\mathbf{S}^{\text{curl}} = -\frac{1}{4\pi} \nabla \int_{V'} \frac{\nabla' \cdot \mathbf{S}(\mathbf{r}')}{|\mathbf{r} - \mathbf{r}'|} d\mathbf{r}' \quad (3)$$

Importantly, the Helmholtz' theorem can be extended to a vector field defined on the open or closed surface using surface divergence and gradient operators.

After the EM field has been solved through various methods or tools [4], by inserting an artificial testing plane (simply connected) at proper position, we can obtain the field and equivalent sources for EM analysis. Hence, we will focus on the decomposition of the equivalent surface current. On a simply connected surface, the decomposition of the surface current can be represented by scalar potentials ϕ and θ [5]

$$\mathbf{S}_s = \mathbf{S}_s^{\text{curl}} + \mathbf{S}_s^{\text{div}} = \nabla_s \phi + \hat{\mathbf{n}} \times \nabla_s \theta \quad (4)$$

where $\hat{\mathbf{n}}$ is the unit vector normal to the surface, ∇_s is the surface gradient operator, and ϕ and θ are scalar potentials corresponding to $\mathbf{S}_s^{\text{curl}}$ and $\mathbf{S}_s^{\text{div}}$, respectively. They correspond to the capacitive and inductive physics entangled in the total surface current \mathbf{S}_s . They can be uniquely determined by the following surface Poisson equations

$$\nabla_s^2 \phi = \nabla_s \cdot \mathbf{S}_s \quad (5)$$

$$\nabla_s^2 \theta = \nabla_s \cdot (\mathbf{S}_s \times \hat{\mathbf{n}}) \quad (6)$$

For an arbitrary curved surface, finding the inverse of the surface Laplace operator ∇_s^2 in (5) and (6), which is called Laplace-Beltrami operator, is extremely difficult in contrast to the inverse of the volume Laplace operator ∇^2 [6]. However, for the vector field defined on a planar surface, ϕ in (5) can be solved by the following IE with the 2D electrostatic Green's function

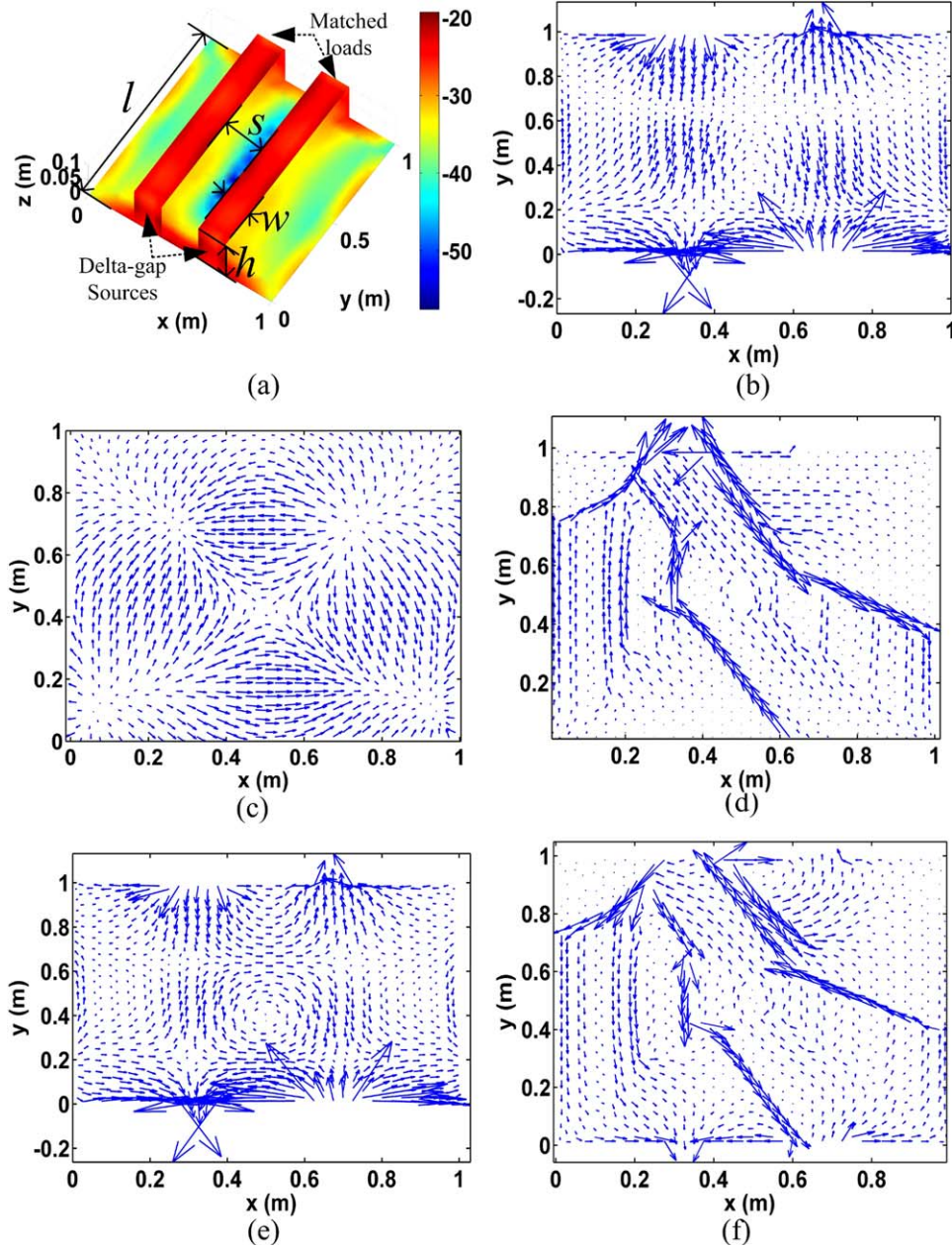


Figure 2 The HD for the CTLs operating at the odd mode. (a) The geometry and amplitude of the surface currents. $l = 1.0$ m, $w = 0.15$ m, $h = 0.1$ m, and $s = 0.2$ m. The working frequency $f = 300$ MHz; (b) the total current on the ground plane; (c) the CF component; (d) the tree current component; (e) the DF component; (f) the loop current component. [Color figure can be viewed in the online issue, which is available at wileyonlinelibrary.com]

$$\phi = -\frac{1}{2\pi} \int_S \frac{\nabla_s \cdot \mathbf{S}_s(\mathbf{r}')}{\ln |\mathbf{r} - \mathbf{r}'|} dS' \quad (7)$$

The Eq. (7) is essentially a convolution and can be accelerated by the efficient fast Fourier transform method.

Hence, the HD process can be implemented as follows. Suppose EFIE is solved based using Rao-Wilton-Glisson basis functions [7]. From the resultant surface electric current \mathbf{J}_s , the equivalent sources on the given testing surface can be computed by

$$\mathbf{J}_s^e = \hat{\mathbf{n}} \times \nabla \times \int_S \overline{\mathbf{G}}(\mathbf{r}, \mathbf{r}') \cdot \mathbf{J}_s(\mathbf{r}') d\mathbf{r}' \quad (8)$$

$$\mathbf{M}_s^e = -i\omega\mu\hat{\mathbf{n}} \times \int_S \overline{\mathbf{G}}(\mathbf{r}, \mathbf{r}') \cdot \mathbf{J}_s(\mathbf{r}') d\mathbf{r}' \quad (9)$$

where $\overline{\mathbf{G}} = (\overline{\mathbf{I}} + \frac{\nabla\nabla}{k^2}) \frac{e^{ik|\mathbf{r}-\mathbf{r}'|}}{4\pi|\mathbf{r}-\mathbf{r}'|}$ is the 3D dyadic Green's function, ω is the angular frequency of interest, and μ is the permeability of free space. Next, the scalar potential ϕ for the equivalent current \mathbf{J}_s^e or \mathbf{M}_s^e can be assessed by the IE (7). Then, the CF component can be computed by taking the gradient of ϕ , which can be further imposed on the 2D electrostatic Green's function, that is,

$$\mathbf{J}_s^{\text{curl}} = -\frac{1}{2\pi} \int_S \nabla_s \left(\frac{1}{\ln |\mathbf{r} - \mathbf{r}'|} \right) \nabla_s \cdot \mathbf{J}_s^e(\mathbf{r}') dS' \quad (10)$$

Finally, the DF current can be evaluated by

$$\mathbf{J}_s^{\text{div}} = \mathbf{J}_s - \mathbf{J}_s^{\text{curl}} \quad (11)$$

2.2. HD and the Loop-Tree Decomposition

It is popular to decompose low-frequency surface current densities into loop-tree basis as discussed in [8]

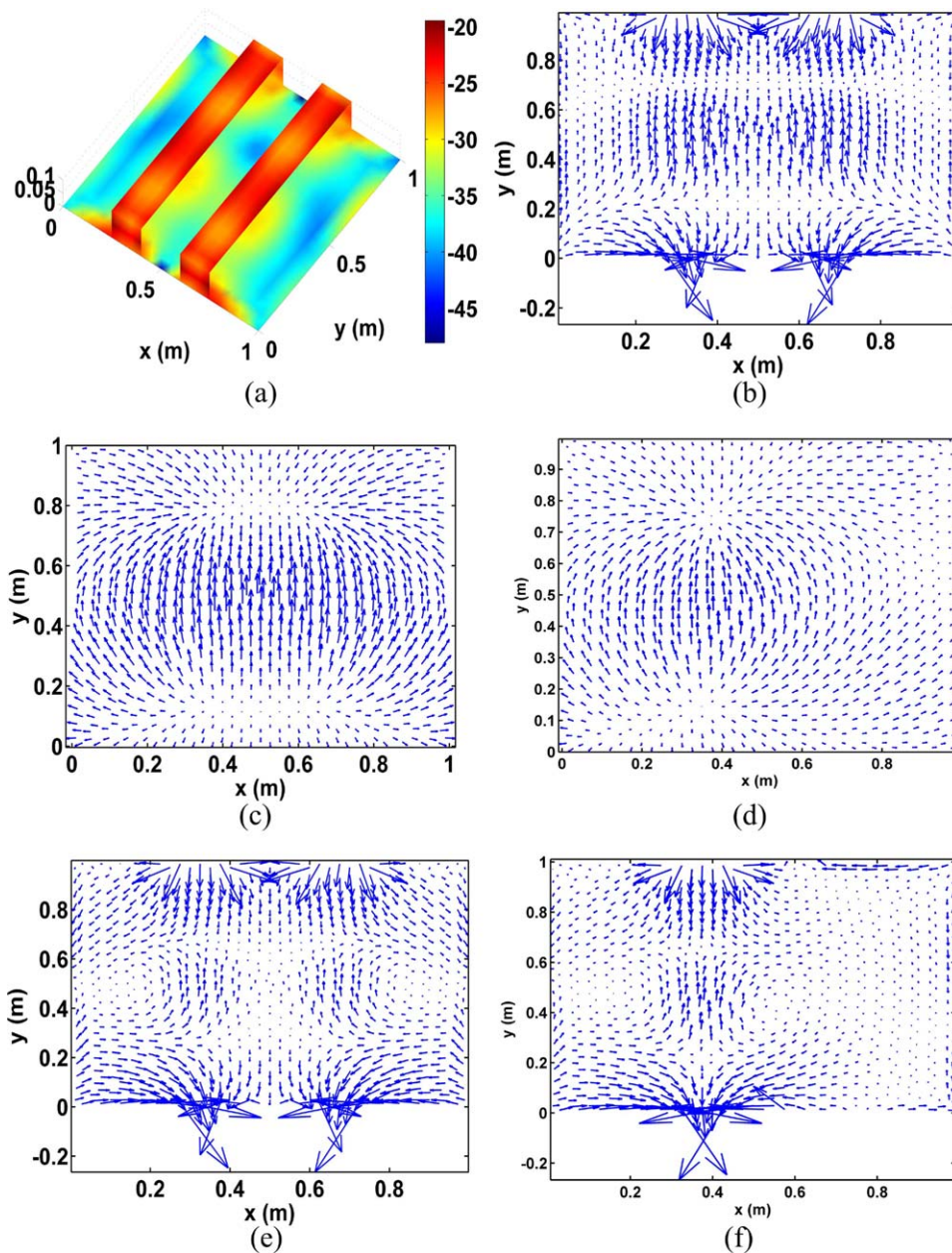


Figure 3 The HD for the CTLs operating at the even mode and mixed mode. (a) The amplitude of even mode surface currents; (b) the total even mode current on the ground plane; (c) the even mode CF component; (d) the mixed mode CF component; (e) the even mode DF component; (f) the mixed mode CF current component. [Color figure can be viewed in the online issue, which is available at wileyonlinelibrary.com]

$$\mathbf{J}_s = \mathbf{J}_{\text{tree}} + \mathbf{J}_{\text{loop}} \quad (12)$$

However, there are several significant differences between the loop-tree decomposition and the proposed decomposition.

First, the loop-tree is the quasi-Helmholtz-decomposition. Even though the loop basis is divergence free ($\nabla \cdot \mathbf{J}_{\text{loop}} = 0$), the tree basis is not curl free ($\nabla \times \mathbf{J}_{\text{tree}} \neq 0$). Hence, the current by tree basis does not correctly depict the irrotational portion and it is not unique. However, the proposed rigorous HD process provides the unique irrotational current and works for all frequency. This is demonstrated in the Benchmark *B* of Section 3.

Second, the loop-tree method was more frequently used for the field calculation. The information is usually consolidated together after both tree and loop currents are obtained. However, the proposed HD in this article is specially for the EM field data analysis to extract and visualize vital EM field property. It

is possible to be used in the field calculation process, which is the result of another project.

At the end, the loop-tree is an effective low-frequency method for the low-frequency regime. It is not effective when the frequency goes high. Hence, examination of the irrotational and solenoidal parts of the field or currents based on the loop-tree method will cause confusing result at high frequencies. But the proposed HD works for all frequencies. Hence, we can avoid messy decomposed current components as shown in the Benchmark *B* of Section 3.

3. NUMERICAL RESULTS

3.1. Fictitious Current on a Planar Surface

The first example is dedicated for the algorithm verification. The fictitious vector current on a planar surface with the size of 1×1 can be decomposed analytically

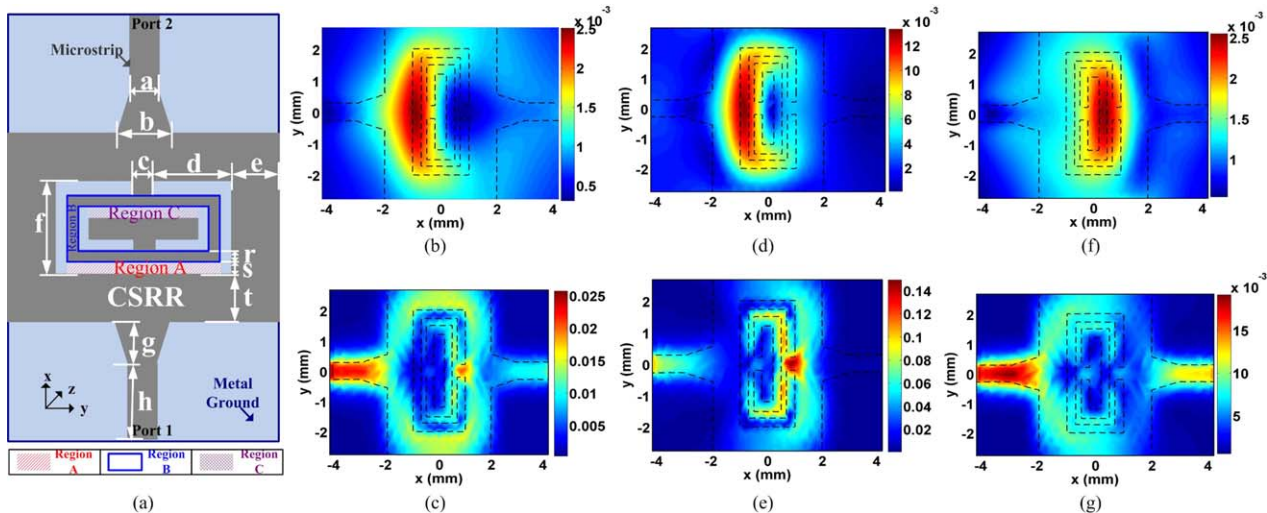


Figure 4 The HD for a microstrip patch incorporated with a CSRR. (a) The schematic pattern. The geometry is set as follows: $b = 2a = 1.12$ mm, $c = 2r = 0.4$ mm, $d = 1.8$ mm, $f = 2e = 2g = 2t = 2.0$ mm, $h = 1.5$ mm and $s = 0.3$ mm. (b,c) The CF and DF currents at the off-resonance frequency of 11 GHz; (d,e) The CF and DF currents at the resonance frequency of the CSRR; (f,g) The CF and DF currents at the off-resonance frequency of 18.8 GHz. [Color figure can be viewed in the online issue, which is available at wileyonlinelibrary.com]

$$\mathbf{J}_s^{\text{div}} = \mathbf{e}_x \sin(kx)^2 \sin(2ky) - \mathbf{e}_y \sin(2kx) \sin(ky)^2 \quad (13)$$

$$\mathbf{J}_s^{\text{curl}} = \mathbf{e}_x \sin(2kx) \sin(ky)^2 + \mathbf{e}_y \sin(kx)^2 \sin(2ky) \quad (14)$$

where $k = 2\pi/\lambda$ is the wave number. Figure 1(a) shows the original current \mathbf{J}_s on the surface. The CF and DF currents calculated by the SIE method are illustrated in Figures 1(b) and 1(c), respectively. Figure 1(d) shows the relative error of the CF current as a function of points per unit through comparing the analytical solution (14) with the SIE result.

3.2. Coupled Transmission Line

The proposed decomposition method can be used to provide more insight about the field radiation than the total current or field. One of its applications is to identify EM interference sources and their properties. The canonical problem is to analyze the return current on the ground plane for coupled transmission lines (CTLs) under different working modes, as shown in Figures 2 and 3. Figure 2 shows the analysis for the odd (differential) mode excitation, where the voltages are set to +1 V and -1 V for the two input ports, respectively. If both voltages are set to +1 V and +1 V, we can obtain the result of the even (common) mode, as shown in Figures 3(a)–3(c), and 3(e). If they are set to +1 V and 0 V, we can obtain the result of the mixed mode, as shown in Figures 3(d) and 3(e).

By comparing Figures 2(c) and 2(e) and Figures 2(d) and 2(f), clearly the proposed HD process produces much reasonable irrotational and solenoidal current than the tree and loop current distribution on the ground plane.

In Figure 3(c), the decomposed CF component from the proposed method shows a very strong dipole moment that contributes greatly to the common mode radiation. Hence, the common mode propagation is expected to have the representative property of the electric dipole radiation. The CF component of the odd mode in Figure 2(c) has two pairs of opposite electric dipoles. Therefore differential signal demonstrates much weaker electrical radiation. By checking the DF components in Figure 2(e) and Figure 3(e), magnetic dipole radiations are also weak due to the cancelation of

the solenoidal loop current's radiation. From another point view, because the far field EM emission can be simply written as $\mathbf{E}_{\text{far}}(\mathbf{r}) = \mathbf{E}_{\text{far}}^{\text{curl}}(\mathbf{r}) + \mathbf{E}_{\text{far}}^{\text{div}}(\mathbf{r})$, where

$$\mathbf{E}_{\text{far}}^{\text{curl,div}}(\mathbf{r}) = \frac{\omega\mu\epsilon e^{ikr}}{4\pi r} \int_S e^{-ik\cdot\mathbf{r}'} (\bar{\mathbf{I}} - \hat{\mathbf{k}}\hat{\mathbf{k}}) \cdot \mathbf{J}_s^{\text{curl,div}}(\mathbf{r}') dS' \quad (15)$$

For circuit EMI problems, the objects' dimensions are usually a very small fraction of the working wavelength. The $\mathbf{E}_{\text{far}}^{\text{div}}$ has much smaller radiation compared to the $\mathbf{E}_{\text{far}}^{\text{curl}}$ if the magnitude of $\mathbf{J}_s^{\text{div}}$ is comparable to $\mathbf{J}_s^{\text{curl}}$. Hence, from the HD result, we could effectively estimate which radiation (electric dipole or magnetic dipole) is dominant.

From the mixed mode CF and DF current distributions in Figures 3(d) and 3(f), we can tell that the electric dipole moment is in between the odd mode and the even mode. Hence, its EM emission is also in between those two cases.

3.3. Complementary Split-ring Resonator

The third example is to use the proposed HD to analyze a resonating structure that is important for RF and microwave circuit modeling. The complementary split-ring resonator (CSRR) [9] shows an effective negative permittivity in microstrip devices. Having exotic properties and broad applications, the CSRR is a key element for the metamaterial design in microwave engineering. The subwavelength CSRR can be modeled as a LC resonant circuit with strong quasistatic features. Here its capacitive and inductive responses are modeled using the HD. Figure 4(a) shows the layout of the CSRR etched in the top layer. The ground plane occupies 9.0×6.0 mm². Air is used as a substrate with the height of 0.254 mm. The tapered transition (lead) can adiabatically transform the energy of the microstrip line to the CSRR. Three frequency points are considered involving the resonance frequency at 13 GHz with a stop-band characteristic, and the two off-resonance frequencies at 11 and 18.8 GHz with the same insertion loss of 5 dB. Figures 4(b), 4(d), and 4(f) and 4(c), 4(e), and 4(g) show the CF and DF currents at the frequencies of 11, 13, and 18.8 GHz, respectively. First, we notice that

the CF currents are much smaller than the DF ones for all the frequencies, which agrees with the quasistatic feature of the CSSR. Second, the resonance of the CSSR satisfies the Lorentz oscillator model. Consequently, both the CF and DF currents reach their maxima as illustrated in Figures 4(d) and 4(e). Additionally, the DF currents at the right-hand side lead undoubtedly confirm the band stop feature of the CSSR. Third, the CF currents corresponding to the capacitive response of the CSSR are concentrated at the air slot regions of A and C denoted in Figures 4(a). While the DF currents in Figures 4(c) and 4(e) corresponding to the inductive response of the CSSR are trapped at the metallic strip region B denoted in Figure 4(a). Interestingly, the peaks of the CF currents tunnel from the region A to the region C as the frequency increases as shown in Figures 4(b), (d), and 4(f). In comparison with the outer air slot related to the region A, the inner one related to the region C has smaller capacitance value.

4. CONCLUSION

An IE-based rigorous HD process is proposed to extract and analyze the EM field. It provides much clearer insight into field coupling and radiation mechanisms. Compared to the loop-tree based decomposition, it is rigorous and frequency-independent. This method provides a novel angle and a powerful postprocessing facility to reproduce and understand the complex EM responses for EMI/EMC, antennas, SI, and other areas.

ACKNOWLEDGMENTS

This work was supported in part by the Research Grants Council of Hong Kong (GRF 711511, 713011, and 712612), HKU Small Project Funding (201007176196), HKU Seed funding (201102160033), NSFC 61271158, and in part by the University Grants Council of Hong Kong (Contract No. AoE/P-04/08).

REFERENCES

1. H. Helmholtz, *Über Integrale der hydrodynamischen Gleichungen welche den Wirbelbewegungen entsprechen*, *J Reine Angew Math* 55 (1858), 25–55.
2. F. Petronetto, A. Paiva, M. Lage, G. Tavares, H. Lopes, and T. Lewiner, *Meshless Helmholtz-Hodge decomposition*, *IEEE Trans Vis Comput Graph* 16 (2010), 338–349.
3. Y.Y. Tong, S. Lombeyda, A.N. Hirani, and M. Desbrun, *Discrete multiscale vector field decomposition*, *ACM Trans Graph* 22 (2003), 445–452.
4. W.C. Chew, M.S. Tong, and B. Hu, *Integral Equation Methods for Electromagnetic and Elastic Waves*, Morgan & Claypool, London, UK, 2009.
5. J.V. Bladel, *Electromagnetic fields*, 3rd ed, IEEE Press, New York, NY, 2007, pp. 1018–1027.
6. C.L. Epstein and L. Greengard, *Debye sources and the numerical solution of the time harmonic Maxwell equations*, *Commun Pur Appl Math* 63 (2010), 413–463.
7. S.M. Rao, D.R. Wilton, and A.W. Glisson, *Electromagnetic scattering by surfaces of arbitrary shape*, *IEEE Trans Antennas Propag* 30 (1982), 409–418.
8. J.S. Zhao and W.C. Chew, *Integral equation solution of Maxwell's equations from zero frequency to microwave frequencies*, *IEEE Trans Antennas Propag* 48 (2000), 1635–1645.
9. M.Q. Lin and T.J. Cui, *Controlling the bandwidth of split ring resonators*, *IEEE Microwave Wireless Compon Lett* 18 (2008), 245–247.

COMPACT SINGLE-LAYER CIRCULARLY POLARIZED ANTENNA FOR SHORT-RANGE COMMUNICATION SYSTEMS

Ornella Leonardi,¹ Mario Giuseppe Pavone,² Gino Sorbello,¹ Andrea Francesco Morabito,³ and Tommaso Isernia³

¹Department of Electrical Electronics and Computer Engineering, Catania University, Viale A. Doria 6, 95125 Catania, Italy; Corresponding author: gino.sorbello@dieei.unict.it

²ST Microelectronics, Stradale Primo Sole 50, 95125 Catania, Italy

³Department of Information Infrastructure and Sustainable Energy Engineering, Mediterranean University of Reggio Calabria, Via Graziella, Loc. Feo di Vito, 89122 Reggio Calabria (RC), Italy

Received 20 December 2013

ABSTRACT: *Dedicated short-range communications (DSRCs) is a short-to-medium range wireless protocol designed for automotive systems. This article describes the development of a one-layer compact left-hand circularly polarized antenna with a footprint and characteristics suitable for on-board-unit antenna of a DSRC system. The size of the developed prototype is $40 \times 40 \times 1.55 \text{ mm}^3$ and exhibits a circularly polarized gain of about 4.68 dBi with a cross polarization discrimination of about 22.5 dB. © 2014 Wiley Periodicals, Inc. *Microwave Opt Technol Lett* 56:1843–1846, 2014; View this article online at wileyonlinelibrary.com. DOI 10.1002/mop.28453*

Key words: *left-hand circularly polarized antennas; dedicated short-range communication; on-board unit; patch antenna*

1. INTRODUCTION

Dedicated short-range communication (DSRC) systems provide a high-speed radio link between road side equipment (RSE), a fixed unit placed on a road infrastructure, and on-board equipment/unit (OBE/OBU), a mobile unit placed inside the vehicle, within a small communication range (up to 1000 m in optimal weather condition).

The OBU market for electronic toll collection is rapidly increasing and spreading to several countries and can be estimated around 1 ML/year due to the large number of OBU devices required. However, the single OBU needs to be reasonably priced and an appropriate antenna for the RSE needs to be simple, compact, and low cost.

In Europe, the EN12253 standard [1] specifies the requirements for the communication between RSE and OBU at 5.8 GHz and the OBU antenna features. The OBU antenna should

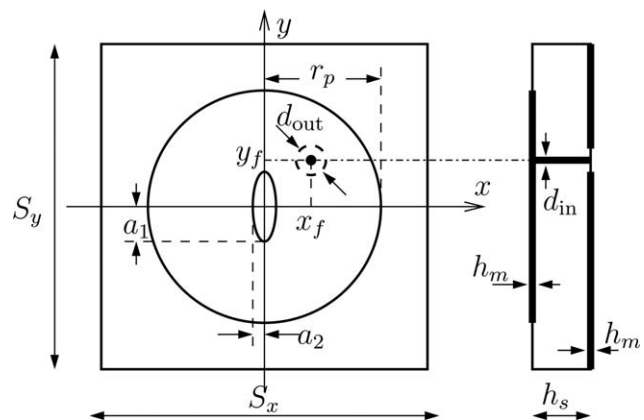


Figure 1 Antenna layout front and side views. A continuous line is used for the patch, while a dashed line is adopted for guard ring on the ground plane